

Functional assay and structure–activity relationships of new third-generation P-glycoprotein inhibitors

Henrik Müller,^a Ilza K. Pajeva,^{a,b} Christoph Globisch^a and Michael Wiese^{a,*}

^a*Institute of Pharmacy, University of Bonn, An der Immenburg 4, 53121 Bonn, Germany*

^b*Center of Biomedical Engineering, Bulgarian Academy of Sciences, Acad. G. Bonchev Str. Bl. 105, 1113 Sofia, Bulgaria*

Received 10 August 2007; revised 15 November 2007; accepted 21 November 2007

Available online 28 November 2007

Abstract—Twenty-eight compounds, including 24 structurally related derivatives of tariquidar synthesized in our laboratory, and four XR compounds, reported by Xenova group Ltd, were investigated by the Hoechst 33342 and Calcein AM functional assays for estimation of their inhibitory effects on the transport activity of P-glycoprotein (P-gp). A high correlation between the effects obtained in both assays was observed at the substrate concentrations used. The analyses of kinetics data from experiments at different substrate concentrations revealed non-competitive inhibition in the Calcein AM assay and competitive inhibition in the Hoechst 33342 assay. The 3D structures of the compounds were further aligned on Hoechst 33342 using flexible and pharmacophore alignments. The results suggested that inhibitors could interact with the H-binding site of P-gp and this could potentially be achieved by different ways of binding. The best 3D-QSAR models, generated by CoMFA and CoMSIA, yielded an internal predictive squared correlation coefficient higher than 0.8 and included electrostatic, steric, hydrogen bond acceptor, and hydrophobic fields. Validation of the models on an external test set of 30 XR compounds gave predictive squared correlation coefficients of up to 0.66. An excellent correspondence between the experimental and modeled activities of the test compounds was observed. The models can be used for prediction and rational design of new P-gp inhibitors.

© 2007 Elsevier Ltd. All rights reserved.

1. Introduction

P-glycoprotein (P-gp) associated multidrug resistance (MDR) is one of the major forms of resistance in cancer cells. P-gp actively transports a number of structurally different compounds out of the tumor cells. Since the discovery of P-gp¹ in 1976 a lot of investigations have been performed to understand its drug efflux function and to develop specific and effective P-gp inhibitors. Nowadays, third-generation MDR modulators as tariquidar (XR9576), zosuquidar (LY335979), and others are in the focus of interest.² They have been developed through the use of combinatorial chemistry and structure–activity relationships.³ In contrast to the second-generation modulators, these inhibitors are not substrates of cytochrome P450A4 and thus, they do not alter significantly the pharmacokinetic profiles of co-administered drugs.^{2,4} Among the third-generation

representatives, XR9576 is one of the most potent modulators.^{5,6} It specifically inhibits the P-gp transport function⁷ and thus is considered as an appropriate compound for testing the role of this protein in resistant cancer cells.⁸ XR9576 belongs to a series of anthranilamide derivatives, which have been developed and pharmacologically investigated by Xenova group Ltd.^{9,10} These modulators have been reported to bind to the same binding site of P-gp as the substrate Hoechst 33342¹¹ and their 3D structure–activity relationships have recently been studied.^{12,13}

XR9576 has also been used in our laboratory as a basis for a rational design of new MDR modulators, coded as WK-X and WK-Y compounds.^{14,15} In our efforts to better understand the P-gp function, we recently developed a new functional assay of P-gp activity using Hoechst 33342.¹⁶ We investigated several well-recognized P-gp substrates and inhibitors in the new assay, and additionally in the Calcein AM assay, proceeding from the assumption that by these analyses we can get a deeper insight into the binding sites of the compounds and the way of their interaction with the transporter. We found, however, that at the low substrate concentrations

Keywords: P-glycoprotein; Multidrug resistance; Hoechst 33342 assay; Calcein AM assay; Third-generation modulators; Molecular modeling.

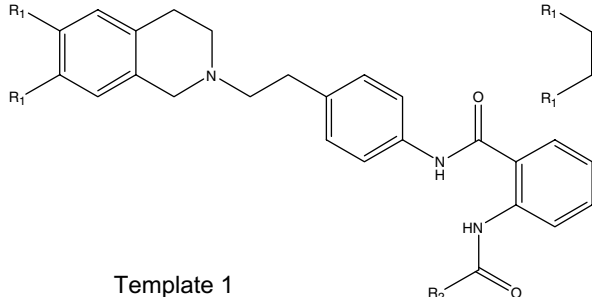
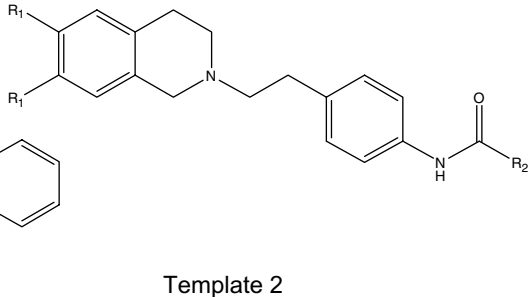
* Corresponding author. Tel.: +49 228 735213; fax: +49 228 737929; e-mail: mwiese@uni-bonn.de

used in the assays, the type of interaction of the compounds with P-gp (competitive or non-competitive) could not be distinguished from the IC_{50} values only.

In this paper we report results of experimental and modeling studies of 24 newly synthesized tariquidar derivatives (WK-X and WK-Y compounds) and four XR-derivatives, 9456, 9544, 9577, and 9504.^{9,10} The compounds have been tested for their potency to inhibit the P-gp transport function using the new Hoechst 33342 assay and the Calcein AM assay. Similarly to the substrates and inhibitors tested previously, we found a good correlation between the IC_{50} obtained by both assays thus confirming once more the conclusion of our previous study.¹⁶ The high correlation between the inhibitory effects did not allow deciding on the type of inhibition and, respectively, on the preferable binding

site of the compounds. To possibly decide on the type of inhibition, additional experiments were performed applying different substrate concentrations. The analyses of the kinetics data derived from these experiments suggest a non-competitive inhibition of Calcein AM and competitive inhibition of Hoechst 33342 transport. Considering these results we further performed molecular modeling of the compounds aiming to get additional information about the way of their interaction with the protein. The molecular modeling shows that the compounds meet the structural and functional requirements for binding to the H-site of the protein. 3D-QSAR models outline the complex role of the electrostatic, steric, hydrophobic, and hydrogen bond (HB) acceptor properties for the inhibitory effect of the tariquidar analogs. The models were validated on an external test set of 30 XR compounds¹⁰ and a very good correspondence be-

Table 1. Structures and activity data of the studied compounds

				
Template 1			Template 2	
Compound	R ₁	R ₂	pIC ₅₀ ± SD (Hoechst 33342)	pIC ₅₀ ± SD (Calcein AM)
Template 1				
XR9456	OCH ₃	Phenyl	6.29 ± 0.06	6.14 ± 0.23
XR9544	OCH ₃	3-Quinoliny	6.78 ± 0.09	6.62 ± 0.26
XR9577	H	3-Quinoliny	6.45 ± 0.07	6.35 ± 0.27
XR9504	OCH ₃	4-Methylphenyl	6.28 ± 0.23	6.16 ± 0.31
WK-X-34	OCH ₃	3,4-Dimethoxyphenyl	6.48 ± 0.15	6.47 ± 0.18
Template 2				
WK-X-14	OCH ₃	2-Nitrophenyl	5.26 ± 0.03	5.32 ± 0.10
WK-X-15	H	2-Nitrophenyl	4.87 ± 0.02	4.91 ± 0.11
WK-X-16	OCH ₃	2-Aminophenyl	4.95 ± 0.24	5.04 ± 0.07
WK-X-17	H	2-Aminophenyl	5.02 ± 0.04	5.03 ± 0.24
WK-X-30	OCH ₃	4-Nitrophenyl	5.86 ± 0.06	5.96 ± 0.14
WK-X-31	H	4-Nitrophenyl	5.30 ± 0.16	5.35 ± 0.13
WK-X-33	OCH ₃	4-Aminophenyl	5.15 ± 0.09	5.39 ± 0.19
WK-X-37	H	4-Aminophenyl	5.38 ± 0.32	4.87 ± 0.21
WK-X-51	OCH ₃	3-Quinoliny	6.84 ± 0.25	6.19 ± 0.10
WK-X-52	H	3-Quinoliny	6.38 ± 0.09	6.28 ± 0.04
WK-X-56	OCH ₃	3,4-Dimethoxyphenyl	5.27 ± 0.25	5.38 ± 0.19
WK-X-57	OCH ₃	4,5-Dimethoxy-2-nitrophenyl	5.31 ± 0.14	5.21 ± 0.34
WK-X-58	OCH ₃	4-Quinoliny	5.65 ± 0.27	5.55 ± 0.33
WK-X-66	OCH ₃	Benzo-1,3-dioxole	5.85 ± 0.19	5.71 ± 0.11
WK-Y-1	OCH ₃	2-Bromophenyl	5.46 ± 0.54	5.37 ± 0.24
WK-Y-2	OCH ₃	3-Bromophenyl	5.49 ± 0.63	5.64 ± 0.23
WK-Y-3	OCH ₃	4-Bromophenyl	5.61 ± 0.37	5.50 ± 0.22
WK-Y-25	OCH ₃	1-Naphthyl	5.73 ± 0.18	5.85 ± 0.12
WK-Y-26	OCH ₃	2-Naphthyl	6.11 ± 0.37	6.11 ± 0.11
WK-Y-27	OCH ₃	2-Quinoxaliny	6.68 ± 0.16	6.31 ± 0.04
WK-Y-28	OCH ₃	3-Isoquinoliny	6.11 ± 0.20	6.07 ± 0.18
WK-Y-29	OCH ₃	3-Pyridyl	5.50 ± 0.23	5.38 ± 0.05
WK-Y-30	OCH ₃	6-Quinoliny	6.13 ± 0.21	6.14 ± 0.16
Verapamil			5.18 ± 0.25	5.34 ± 0.24
Cyclosporin A			5.85 ± 0.05	5.85 ± 0.09

tween the experimental and modeled inhibitory effects was observed. The results of this study may contribute to a better understanding of the interactions and structure–activity relationships of this promising class of P-gp inhibitors and direct the rational design of new and improved inhibitors with higher efficacy, potency, and specificity.

2. Results

2.1. Functional assays

Table 1 presents the structures and activity data of the studied compounds. In total 28 substances have been investigated, among them four XR compounds (9456, 9544, 9577, 9504)^{9,10} and 24 originally synthesized tariquidar analogs (WK-X and WK-Y codes).¹⁷ In the table two template structures are shown. Template 1 is the basic structure of the anthranilamide derivatives XR9456, 9544, 9577, 9504, and WK-X-34. Template 2 represents the basic structure of the remaining compounds. All inhibitors contain a tetrahydroisoquinoline-ethyl-phenyl-amide substructure.

The activity data have been obtained by two functional assays using the P-gp substrates Hoechst 33342 and Calcein AM (see Section 4). In Table 1 the inhibitory effects are reported as logarithm of the reciprocal IC_{50} values (pIC_{50}).

Figure 1 shows a plot of the pIC_{50} values of the compounds obtained in the two assays. As seen from the figure there is a very good correlation between the inhibitory effects ($R = 0.946$).

In order to get a deeper insight into the type of inhibition, additional experiments have been performed using different substrate concentrations. To determine the interaction type, the Lineweaver–Burk and Hanes–Woolf plots were created leading to identical conclusions. Figure 2A displays the Hanes–Woolf plot for

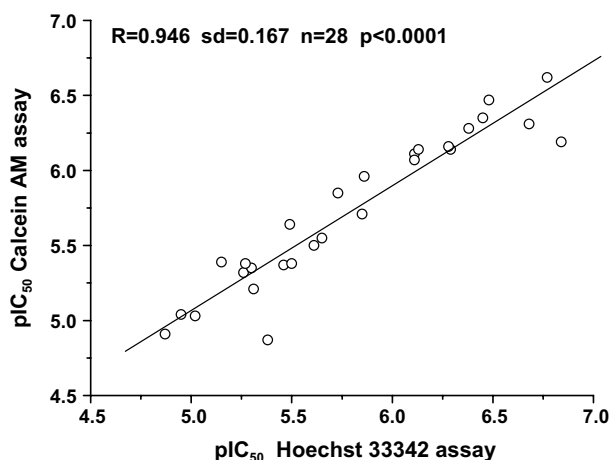


Figure 1. Correlation between the inhibitory effects of the compounds measured in the Hoechst 33342 and Calcein AM assays.

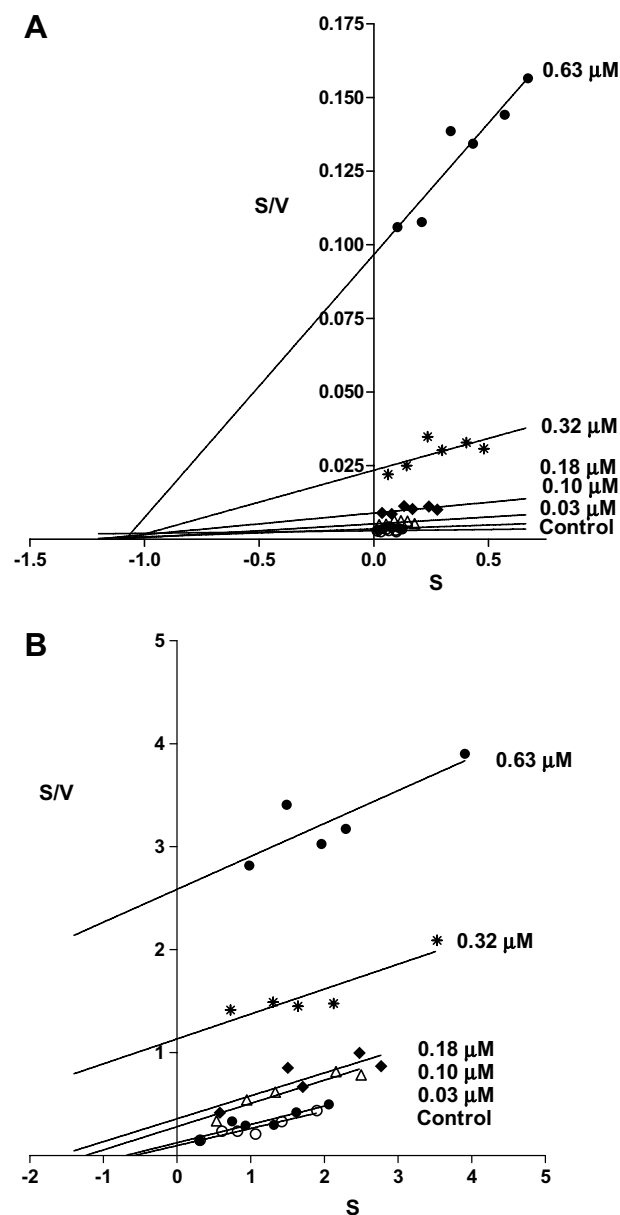


Figure 2. Hanes–Woolf plots for compound WK-X-52: (A) Calcein AM assay; (B) Hoechst 33342 assay.

the inhibitor WK-X-52 based on the Calcein AM data. The characteristics of a non-competitive interaction type between Calcein AM and WK-X-52 are indicated by a common intercept on the negative X-axis. The same plot for WK-X-52 in the Hoechst 33342 assay is shown in Figure 2B. In contrast to Calcein AM the lines are parallel indicating a competitive type inhibition.¹⁸

2.2. Log P correlations

The role of lipophilicity for the inhibitory effect of the MDR modulators was studied using the partition coefficient $\log P$. The $\log P$ values of the compounds were calculated¹⁹ and plotted against activity values. The plots for the Hoechst 33342 (Fig. 3A) and Calcein AM assays (Fig. 3B) are scattered and no distinct correlation

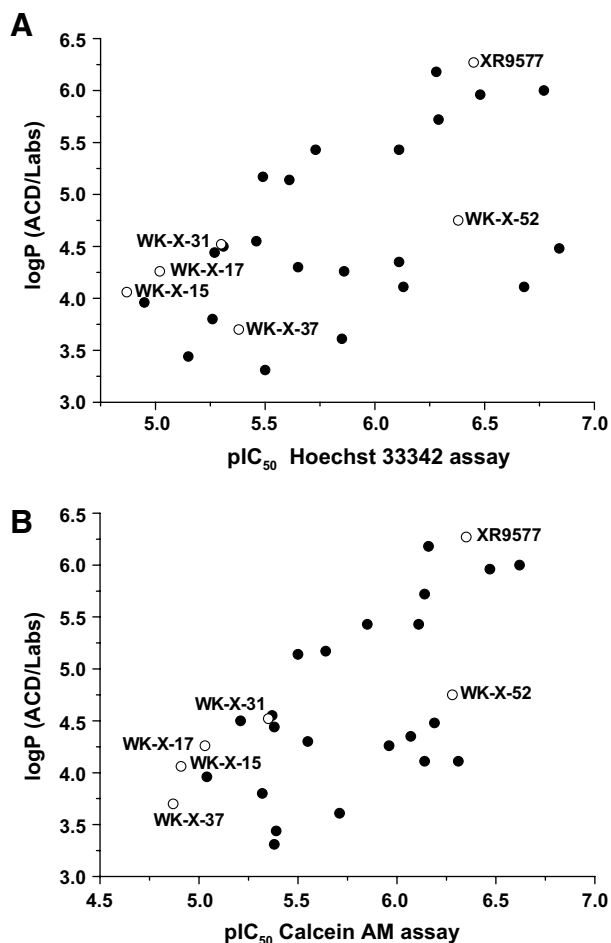


Figure 3. Plot of $\log P$ values calculated with ACD/ $\log D$ ²⁰ versus the inhibitory effect (pIC_{50} values) of all 28 compounds in the Hoechst 33342 assay (A) and Calcein AM assay (B); those compounds that do not contain methoxy groups in position R_1 (Table 1) are shown by open circles.

with $\log P$ can be identified. In the figures the compounds without methoxy groups in R_1 (Table 1) are outlined. Considering that the methoxy groups in R_1 may influence the basicity of the nitrogen atom in the tetrahydroisoquinoline substructure, the compounds' pK_A values were calculated with the program ACD.¹⁹ Results show that the methoxy groups decrease the pK_A value and thus increase the unprotonated form under physio-

logical conditions (pH 7.4). The altered distribution of these substances from the aqueous to the lipid membrane phase has been considered by calculating the $\log D$ values at pH 7.4. Again no distinct correlation between the $\log D$ values and the activity data could be found (data not shown) and the correlation did not improve when excluding the compounds without methoxy groups.

Also for 32 XR compounds¹⁰, no correlation between $\log P$ and their potency to increase accumulation of daunorubicin in AR 1.0 cells was found.

2.3. Modeling of ligands' overlays

The different templates of the inhibitors (Table 1) do not allow to decide directly on their possible overlay, and, correspondingly, on the way of their interaction with the protein. Therefore, applying the FlexS program,²⁰ we investigated the overlays of the ligands on the structure of Hoechst 33342. We took into consideration two facts: (i) the compounds of template 1 are very similar to tariquidar (all possess an anthranilamide nucleus) and tariquidar has been shown to interact with the binding site of Hoechst 33342¹¹; (ii) the results of our functional assays suggest that the compounds of template 2 are competitive inhibitors of Hoechst 33342.

In the overlays we used the Hoechst 33342 conformation with the lowest heat of formation among the four conformers generated (see Section 4). In this conformer the imidazole nitrogens ($-\text{NH}$ and $=\text{N}-$) in both benzimidazole rings had opposite orientations just as shown in Figure 4. It should be, however, noted that the conformation with the same orientation of $-\text{NH}$ and $=\text{N}-$ in both rings is not to be rejected taking into account the small differences in the heat of formations (about 3 kcal/mol) of the conformers with the opposite and similar orientation. In Figure 4 the pharmacophore points of Hoechst 33342 identified in our previous studies are also shown.^{12,21} In the figure the main pharmacophore pattern of compounds that interact with the H-site is outlined: the hydrophobic points H_1 – H_3 , HB-acceptor A_2 , and HB-donor D_2 .

Generally, no correspondence between the FlexS alignment scores and inhibitory effects of the compounds could be found. This can be explained by the fact that

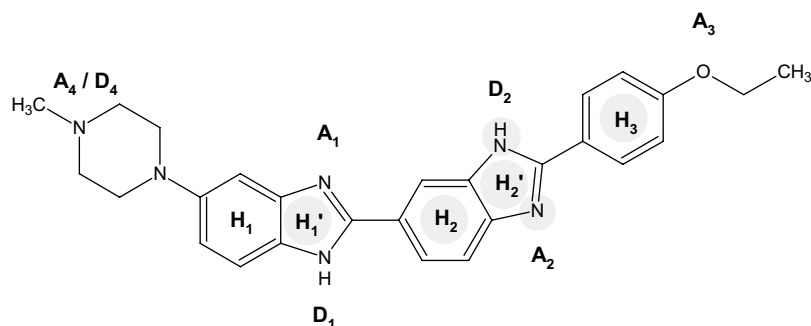


Figure 4. Structure of Hoechst 33342 with the main pharmacophore points identified^{12,22}: H_1 , H_1' , H_2 , H_2' , H_3 —hydrophobic centers; A_1 , A_2 , A_3 , A_4 —HB acceptors; D_1 , D_2 , D_4 —HB donors; the functional groups and atoms involved in the proposed pharmacophore pattern of drugs that interact with the binding site of Hoechst 33342 (H-site) are shaded.

the volume overlap is a component of the scoring function in FlexS.²⁰ The inhibitors based on template 2 (Table 1) produced the highest scores in the overlays due to the good volume overlap; those based on template 1, although highly active, yielded lower scores because of the larger size of their structures compared to Hoechst 33342.

Figure 5 illustrates two typical alignments produced by the anthranilamide derivatives in the series (template 1, Table 1). The mostly observed overlay is illustrated in the example of XR9456 (Fig. 5A). The anthranilamide nucleus of XR9456 is aligned on the ethoxy-phenyl ring of Hoechst 33342 and the R₂ substituent together with the preceding amide group deviate from the substructure overlapped on Hoechst 33342. At the same time there is a very good correspondence between the pharmacophore points H₃, A₂, D₂, and H₂ (Fig. 4) and groups of the same functionality in the XR deriva-

tives. Different orientations were observed in the deviating part of the structure for R₂ (e.g. mirror-like orientation for the quinolinylnyl and substituted phenyl rings) as well as for the amide group (e.g. an orientation opposite to that shown in Fig. 5A). Although not involved in the series, we studied also tariquidar (XR9576) overlays. For XR9576 an alignment was produced similar to that shown in Figure 5A and to the previously identified in our modeling study of the XR derivatives.¹² Again different orientations of the deviating part were obtained suggesting a rather flexible behavior of this substructure. Figure 5B illustrates another alignment produced on the example of XR9544. In this case, compared to Figure 5A, a mirror-like overlay of the whole structure is generated that could potentially correspond to an inverse binding mode. The tetrahydroisoquinoline part is overlaid on the ethoxy-phenyl ring of Hoechst 33342 and the R₂ part of the structure deviates again from the common overlap, this

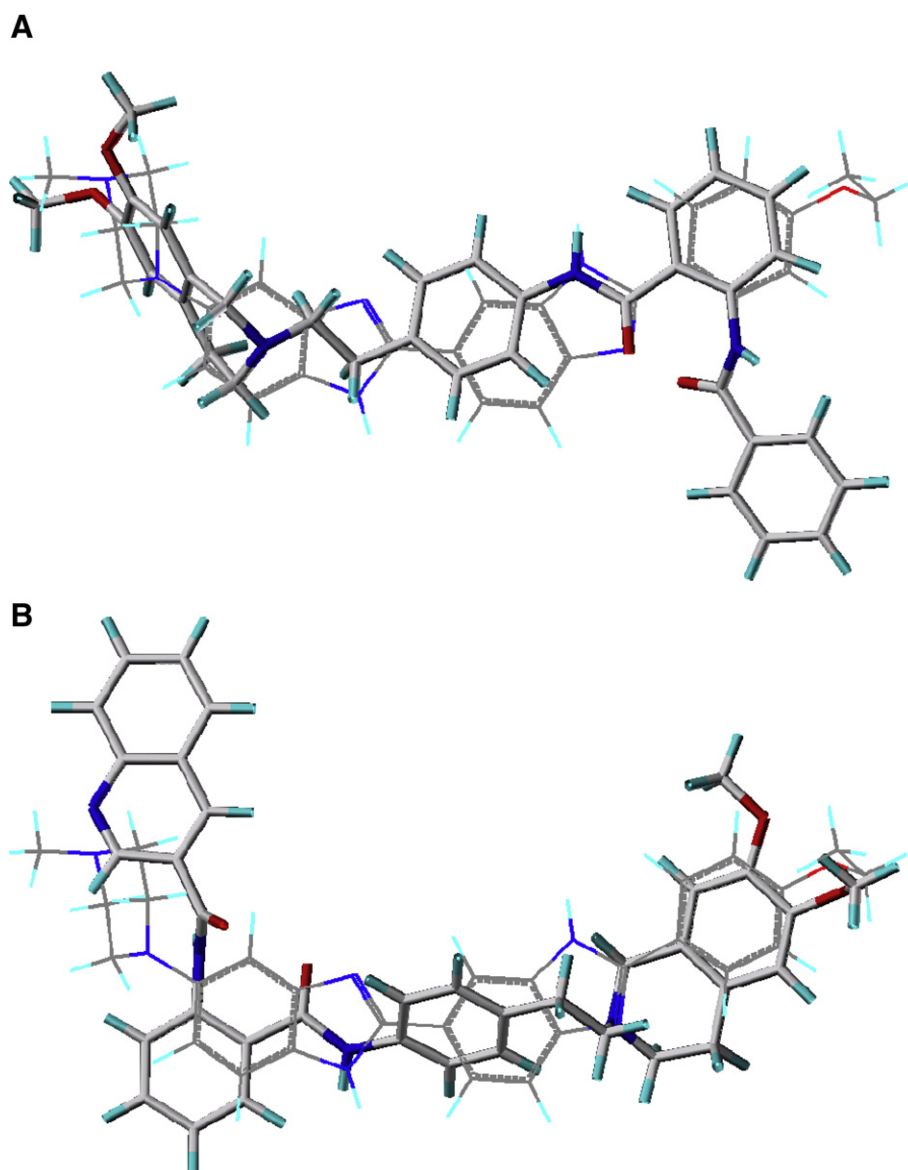


Figure 5. Alignments of the anthranilamide derivatives (structures displayed by sticks) on the lowest energy conformer of Hoechst 33342 (line display); red: O atoms; blue: N atoms; cyan: H atoms; gray: C atoms; (A) XR9456; (B) XR9544.

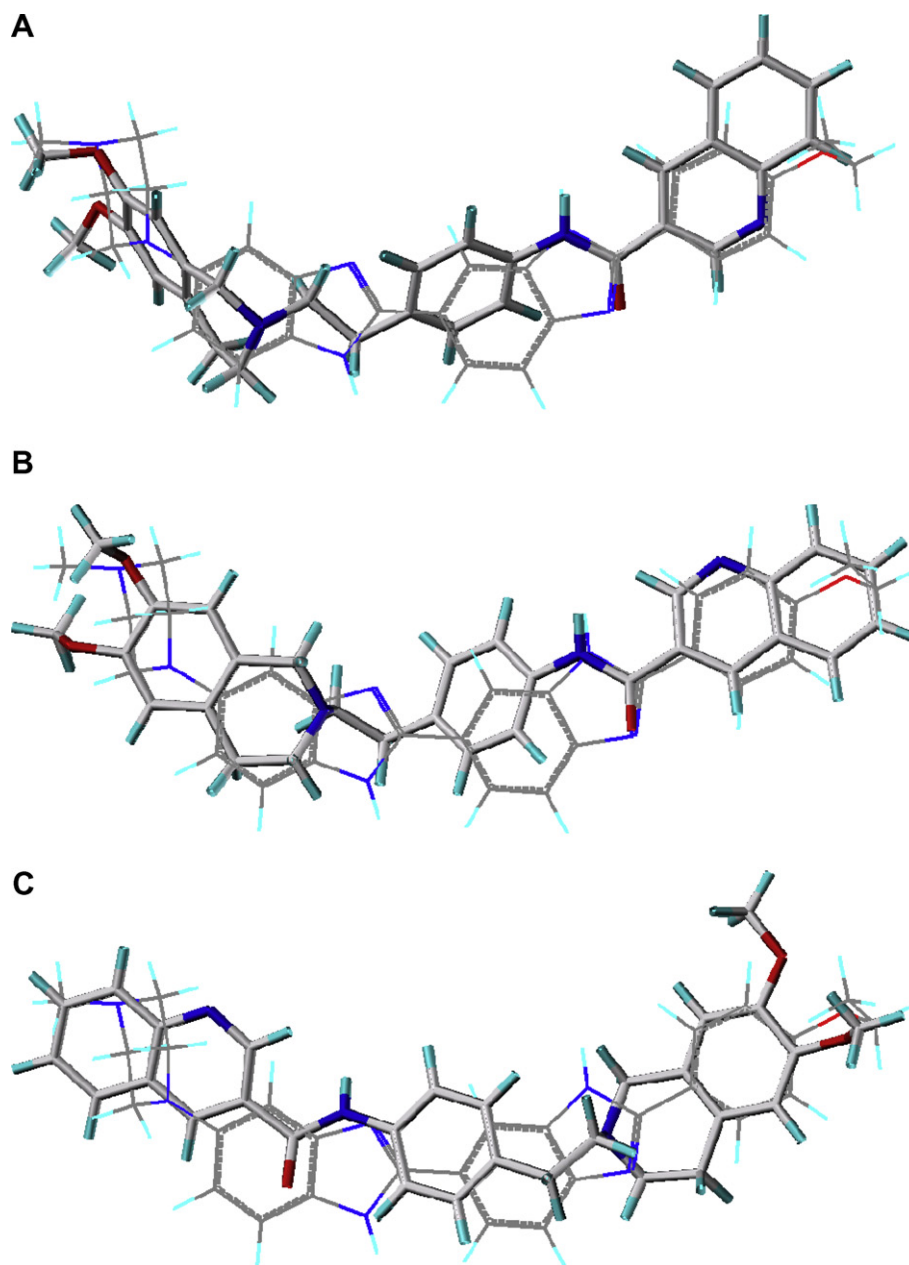


Figure 6. Alignments of WK-X-51 (structures displayed by sticks) on the lowest energy conformer of Hoechst 33342 (line display); red: O atoms; blue: N atoms; cyan: H atoms; gray: C atoms; (A) alignment with quinoline N-atom oriented down; (B) alignment with quinoline N-atom oriented up; (C) alternative alignment.

time at the opposite side. In this overlay a good correspondence to the H₁, H₂, H₃, A₁, and D₁ functional groups of Hoechst 33342 (Fig. 4) is observed and a flexible orientation of R₂ is recorded again. Based on the above overlays and considering the high inhibitory activities of the XR derivatives, it is presumable that the deviating substructure interacts with an additional site on the protein and this interaction is facilitated by its flexibility.

Figure 6 shows the overlays generated with the compound WK-X-51, the most active compound determined in the Hoechst 33342 assay. As seen from the figures good overlaps between both structures are produced. In most cases R₂ was aligned on

the substructure of Hoechst 33342 with the ethoxy-substituted phenyl ring (Fig. 6A and B). The overlays differ by the orientation of R₂: the N atom in the terminal quinoline group may face different directions in relation to the core structure (down or up in Fig. 6A and B, respectively). Independently of the orientation of the quinoline substituent in both alignments, a good correspondence to the pharmacophore points H₂, H₃, A₂, and D₂ (Fig. 4) can be seen.

The above results presume that inhibitors investigated could fit well to the Hoechst 33342 binding site of P-gp and this could be achieved by different ways of binding.

2.4. 3D-QSAR analyses

3D-QSAR analyses were further performed using all 28 compounds (Table 1) as a training set. Considering the differences in the overlays produced by FlexS for the compounds of template 1 and template 2 (Figs. 5 and 6), the alignments were further specified by a pharmacophore alignment on Hoechst 33342, similarly to that applied previously to the XR derivatives.¹² Shortly, the Hoechst 33342 conformers (see Section 4) were used for generation of a set of structural features by applying

the pharmacophore search option in MOE.³³ The compounds were then overlaid on these features using the lowest energy conformers generated by a stochastic search (see Section 4). To decide on the most reasonable orientation of R₂ and considering the FlexS results, overlays with different conformers (from 1 to up to 4 conformers per structure) were systematically explored tracing out their effects on the models generated. The final alignment has been selected based on the highest internal predictivity model and taking into account the consistency of the R₂ orientation.

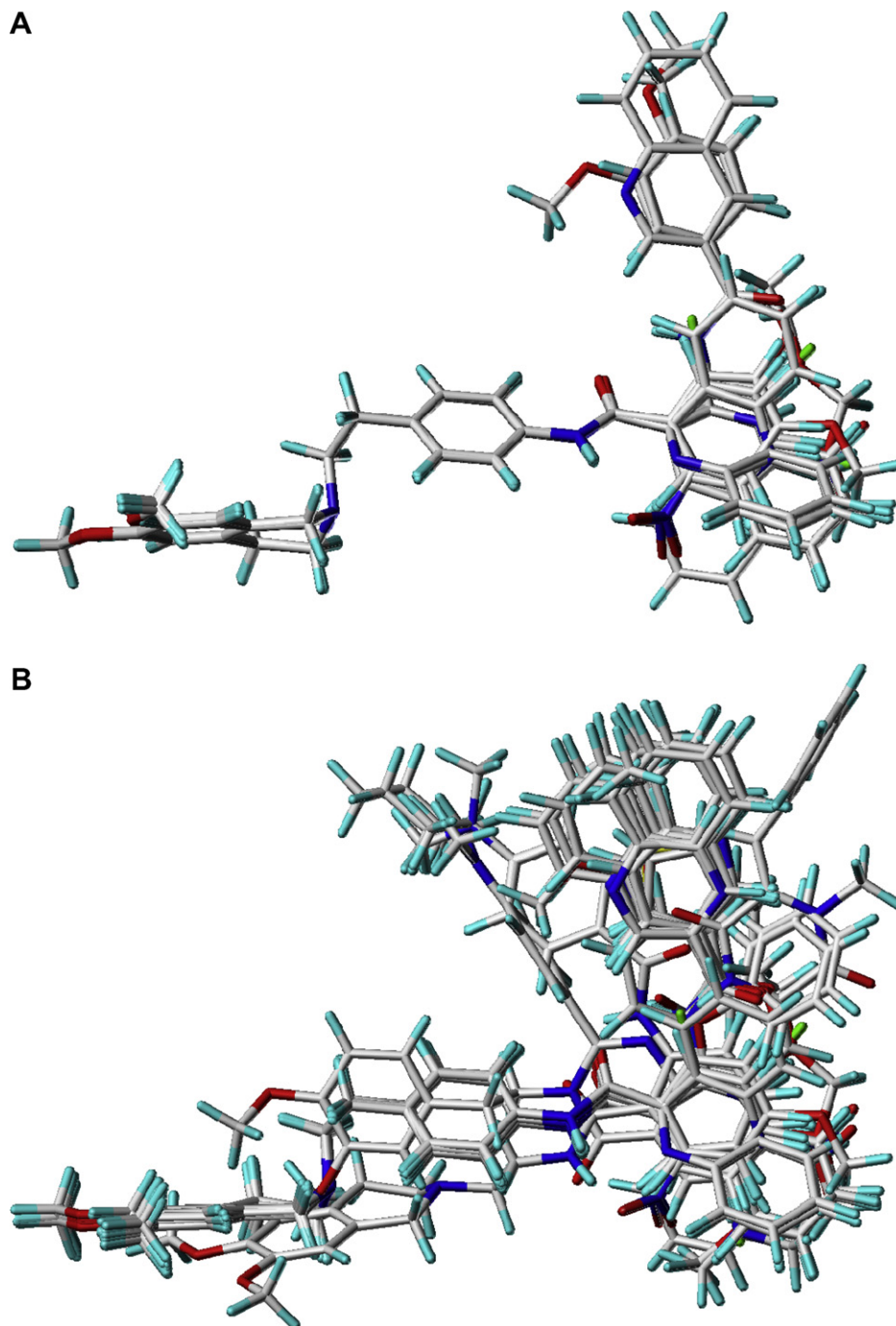


Figure 7. Alignment of the compounds as used in CoMFA and CoMSIA: (A) training set (28 compounds); (B) training (28 compounds) and test sets (30 compounds); red: O atoms; blue: N atoms; cyan: H atoms; gray: C atoms.

Figure 7A illustrates the final alignment of the training set compounds. For the most active compounds of template 1, the –NH– of the amide group attached to R₂ is directed toward the =O atom of the amide group that precedes the anthranilamide ring; the heteroatom in 3-quinoline of XR9544 and XR9577 is ‘left’ oriented. 3-quinolines in the most active compounds of template 2 are oriented as shown in Figure 6A for WK-X-51. This overlay was mostly produced and had the highest scores in the FlexS runs.

As a test set 30 XR compounds described in the paper of Roe et al.¹⁰ have been used for an external validation of the 3D-QSAR models generated. As two of the 32 compounds, XR9456 and XR9544 (Table 1), were involved in the training, they have been excluded from the test set. The test set structures were aligned similarly to the

training set structures. Figure 7B shows the alignment of both training and test set.

The 3D-QSAR analyses were performed using CoMFA and CoMSIA approaches. The span in activity values of the investigated derivatives is approximately two log units (Table 1), thus enabling application of these analyses. Table 2 summarizes the results of the 3D-QSAR models generated with LOO (Leave-One-Out) cross-validation.³⁵ All single fields and all possible combinations of them were calculated. In the table the best models are marked in bold. As seen, the CoMSIA models show better performance on the test set prediction (higher r^2_{pred} and p^2) compared to CoMFA. Additionally, the CoMSIA models have better comparability between q^2 , r^2_{pred} , and p^2 indicating higher stability. In both analyses the best single field model is the electrostatic one, fol-

Table 2. Statistical characteristics of the 3D-QSAR models using CoMFA and CoMSIA obtained in the training and test set runs: the best performing models are shown in bold

Fields	Training						External test			
	LOO			NV			All		w/o 15, 25	
	q^2	S_{PRESS}	n	r^2	s	n	r^2_{pred}	p^2	r^2_{pred}	p^2
<i>CoMFA</i>										
b	0.772	0.313	6	0.964	0.123	6	0.491	0.451	0.614	0.627
b h-bnd	0.657	0.351	2	0.859	0.225	2	0.065	0.119	0.035	0.131
e	0.797	0.295	6	0.969	0.116	6	0.434	0.373	0.587	0.573
e h-bnd	0.542	0.398	1	0.685	0.330	1	−0.049	0.007	−0.069	0.038
h-bnd	0.512	0.410	1	0.649	0.348	1	−0.169	−0.068	−0.207	−0.051
s	0.690	0.341	3	0.869	0.222	3	0.470	0.493	0.535	0.628
s e h-bnd	0.657	0.351	2	0.859	0.225	2	0.065	0.119	0.035	0.131
s h-bnd	0.652	0.377	5	0.961	0.126	5	0.238	0.286	0.233	0.334
<i>CoMSIA</i>										
a	0.525	0.431	4	0.724	0.329	4	0.446	0.430	0.540	0.593
d	0.347	0.485	2	0.434	0.451	2	0.308	0.252	0.363	0.333
d a	0.595	0.398	4	0.811	0.272	4	0.450	0.420	0.533	0.556
e	0.774	0.285	2	0.876	0.211	2	0.485	0.495	0.532	0.599
e a	0.834	0.254	4	0.933	0.162	4	0.581	0.596	0.664	0.754
e d	0.774	0.297	4	0.898	0.200	4	0.486	0.460	0.547	0.563
e h	0.774	0.304	5	0.940	0.157	5	0.442	0.486	0.466	0.570
e h a	0.818	0.273	5	0.950	0.143	5	0.575	0.599	0.642	0.735
e h d	0.751	0.312	4	0.909	0.189	4	0.548	0.516	0.621	0.630
e h d a	0.772	0.299	4	0.918	0.180	4	0.530	0.516	0.610	0.651
h	0.718	0.339	5	0.912	0.190	5	0.007	0.288	−0.069	0.267
h a	0.747	0.321	5	0.905	0.197	5	0.570	0.561	0.650	0.697
h d	0.650	0.370	4	0.805	0.276	4	0.474	0.411	0.566	0.521
h d a	0.674	0.357	4	0.847	0.245	4	0.446	0.404	0.528	0.529
s	0.754	0.317	5	0.915	0.187	5	0.249	0.330	0.315	0.500
s a	0.751	0.319	5	0.913	0.189	5	0.484	0.492	0.586	0.676
s d	0.686	0.358	5	0.904	0.198	5	0.270	0.296	0.345	0.462
s e	0.805	0.289	6	0.957	0.136	6	0.442	0.489	0.495	0.622
s e a	0.832	0.256	4	0.939	0.154	4	0.571	0.590	0.649	0.742
s e d	0.769	0.300	4	0.907	0.190	4	0.512	0.496	0.575	0.606
s e h	0.792	0.292	5	0.940	0.157	5	0.488	0.517	0.532	0.622
s e h a	0.822	0.264	4	0.911	0.186	4	0.543	0.552	0.625	0.724
s e h d	0.759	0.300	3	0.896	0.197	3	0.568	0.529	0.647	0.641
s e h d a	0.777	0.295	4	0.927	0.169	4	0.560	0.547	0.640	0.683
s h	0.760	0.313	5	0.932	0.167	5	0.322	0.421	0.337	0.510
s h a	0.802	0.285	5	0.932	0.167	5	0.552	0.577	0.624	0.724
s h d	0.707	0.331	3	0.851	0.236	3	0.554	0.509	0.639	0.623

Fields: b—both; s—steric; e—electrostatic; h-bnd—hydrogen bonds; h—hydrophobic; a—hydrogen bond acceptor; d—hydrogen bond donor fields. Statistical parameters: q^2 —cross-validated r^2 ; n —optimal number of components; S_{PRESS} —predictive sum of squares; r^2_{pred} —predictive r^2 ; ³⁵ p^2 —predictive squared correlation coefficient of Silverman³⁶; r^2 —squared correlation coefficient; s —standard error of estimate.

lowed by the steric and hydrophobic (in CoMSIA). The combination of the electrostatic with the steric, hydrophobic, and acceptor indices yields the models with best statistical characteristics.

Figure 8A shows the plot of the predicted activity by the 'seha' model versus calculated activity values measured in the Hoechst 33342 assay for the training set compounds. The plot is obtained using the non-validated model generated with four components (Table 2). A good correlation ($r^2 = 0.911$) with an intercept close to zero and a slope close to one is observed. Figure 8B represents the plot of the activities measured in the daunorubicin accumulation assay¹⁰ versus predicted activities in the Hoechst 33342 assay of the test compounds. As seen from the figure two compounds deviate strongly from the line: numbers 15 and 25 (numbers correspond to those used in Ref. 10). It should be noted that compound 15 has not been found in the patent data set⁹ and the activity values of compound 25 (XR9389) differ

significantly in both reference sources (4900 nM¹⁰ and 1800 nM⁹). When excluding these compounds, the prediction improved by 0.1 (Table 2, Fig. 8B). In general, according to the calculated values, the ranking of the compounds is correct as designated by the positions of the most active (XR9576) and the least active (number 7¹⁰ or XR9351⁹) compounds in the test set.

Figure 9 illustrates the contour plots of the 'seha' model for steric and electrostatic (Fig. 9A) and acceptor and hydrophobic fields (Fig. 9B). The contour levels used have been defined based on the distribution of the STDEV * COEFF fields considering the recommendations in Ref. 22

More bulky substituents (Fig. 9A) are favorable in two regions of position R₂ corresponding to template 1 (green contour up) and template 2 (green contour down) compounds. Both regions are outside the volume covered by the pharmacophore of Hoechst 33342 (compare to Figs. 5 and 6) suggesting that the stronger inhibition effect of the compounds requires a more bulky R₂ substructure. Yellow contours of sterically forbidden regions are related to low activity compounds with template 2. The larger favorable steric region overlaps with a small red region of favorable presence of negatively charged substituents. The non-favorable steric region is close to a large blue contour indicating the unfavorable influence of negatively charged substituents. These results reflect the influence of compounds of template 2 containing the phenyl-type R₂ (about half of the training set) that largely vary in the type and the position of the substituents in the phenyl ring. Under these conditions it is reasonable that the electrostatic fields appear to best describe the influence of these substituents and, respectively, the structural variations in the training set.

Figure 9B presents the contour plots of the hydrophobic and HB-acceptor fields. Considering the duality of the hydrophobic fields, the presence of methoxy groups in R₁ is reflected by favorable hydrophilic interactions in this position (violet, Fig. 9B). The same is expected for the region where the unfavorable hydrophobic interactions (violet) are overlapped by favorable HB-acceptor interactions (magenta), thus outlining the importance of the amide group and the nitrogen atom in the heterocyclic R₂ substituents for the inhibition potency of the compounds. The interesting observation is the possibility for favorable HB-acceptor interactions in this part related to either the amide group of the inhibitors of template 1 or the quinoline nitrogen of the strongest representatives of template 2. This suggests that the most active compounds of template 2 could exert their inhibition potency by a HB-acceptor interaction through their quinoline nitrogens with an appropriate amino acid outside the H-site of the protein. Unfavorable HB-acceptor interactions are expected in the cyan-colored parts together with the presence of more hydrophobic substituents (a small orange region, Fig. 9B). This is in agreement with the unfavorable presence of nitro groups in this position (Table 1). The big favorable hydrophobic region (orange, Fig. 9B) characterizes the positive

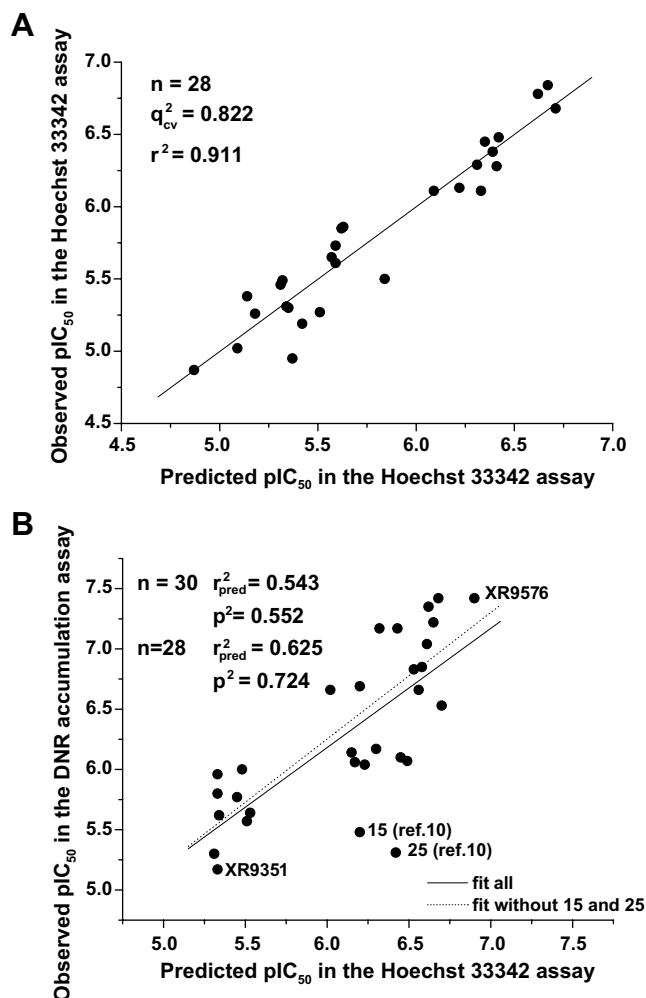


Figure 8. (A) Plot of the observed versus predicted activity values in the Hoechst 33342 assay obtained with the non-validated 3D-QSAR model generated with the 'seha' fields and using LOO cross-validation (Table 2); (B) Plot of the observed activities in daunorubicin (DNR) accumulation assay¹⁰ versus predicted in the Hoechst 33342 assay for the test XR compounds calculated with the same model.

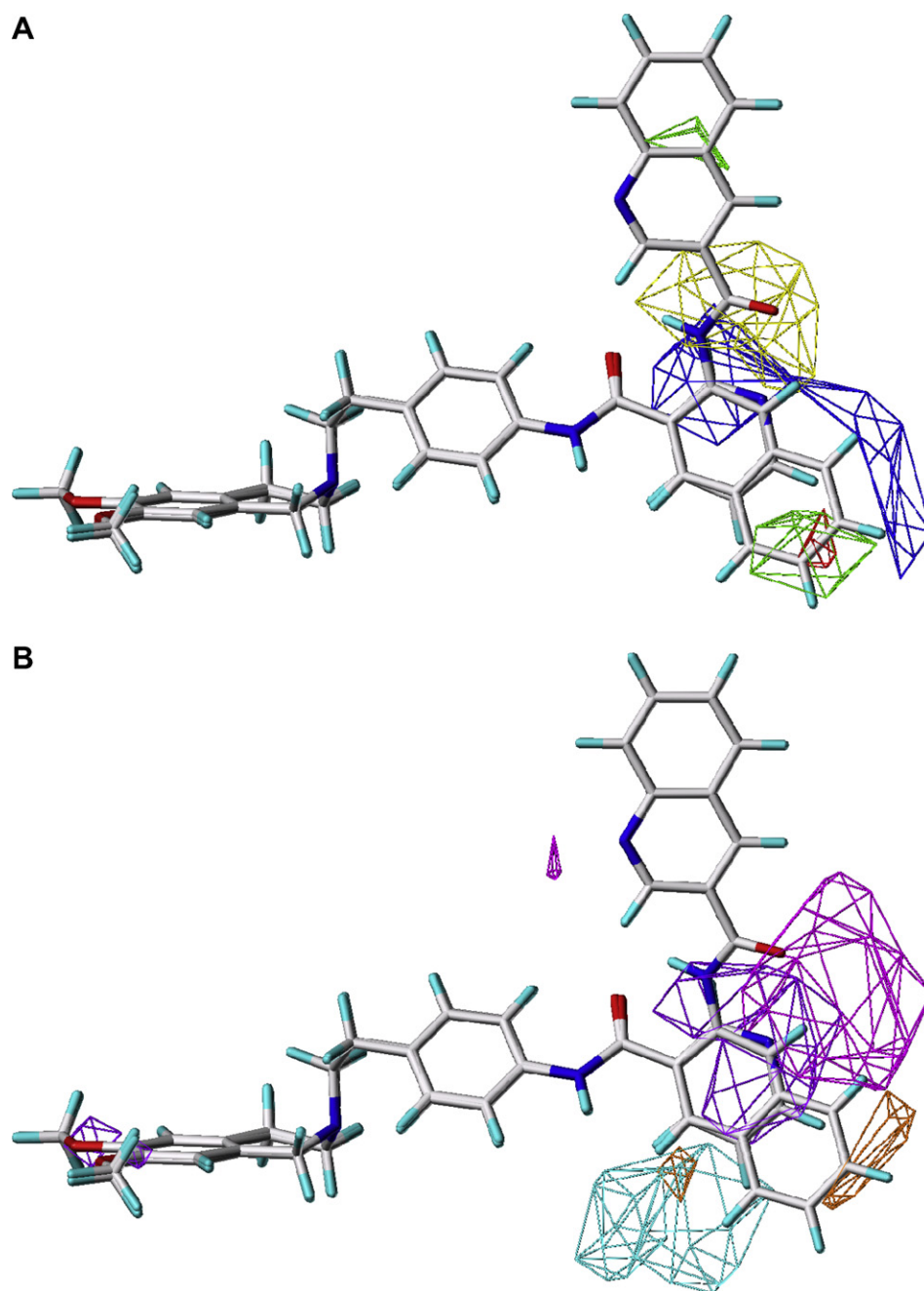


Figure 9. CoMSIA contour plot (STDEV * COEFF) of the 'seha' model (Table 2) with the most active compounds XR9544 (template 1) and WK-X-51 (template 2): (A) steric and electrostatic fields; (B) hydrophobic and acceptor fields. Favorable interactions: green 80% (steric), blue 90% (electrostatic), orange 80% (hydrophobic); magenta 50% (acceptor). Non-favorable interactions: yellow 7% (steric); red 15% (electrostatic); violet 20% (hydrophobic); cyan 4% (acceptor).

influence of the quinoline and para-substituted phenyl compounds of template 2.

3. Discussion

The compounds investigated in this study belong to the third-generation MDR modulators, which are analogs of the powerful P-gp inhibitor XR9576. Five compounds contain an anthranilamide nucleus and all compounds possess in common a tetrahydroisoquinoline-ethyl-phenyl-amide substructure. The main varia-

tions in the series are in the substituents R_1 at the tetrahydroisoquinoline part and in the R_2 part (Table 1). Taking into consideration the experimental errors, the most active compounds in the group, namely WK-X-51, XR9544, WK-Y-27, WK-X-34, XR9577, and WK-X-52, are of comparable potency in both Hoechst 33342 and Calcein AM assays (Table 1).

A high correlation between the inhibitory effects in both assays is observed at the substrate concentrations used (0.3 μ M for Calcein AM and 5 μ M for Hoechst 33342) (Fig. 1). The K_m values determined in the experiments

at different substrate concentrations were 3 μM for Calcein AM and 6 μM for Hoechst 33342, illustrating in this way that the concentrations used in the assays were smaller than the substrate K_m values. These results confirm the suggestion based on theoretical enzyme kinetics models that have been proposed in our previous study: at a substrate concentration well below its K_m value, the type of inhibition (competitive or non-competitive) is unrecognizable in the functional assays¹⁶ and additional measurements are necessary to decide on this. Therefore, the data were further processed by a kinetics analysis applying different kind of linearization plots. The kinetics analyses pointed to non-competitive interaction with Calcein AM and competitive interaction with Hoechst 33342 (Fig. 2) in agreement with the reported competitive interaction of tariquidar and Hoechst 33342.⁷ To our knowledge, this is the first study that shows kinetics analysis of functional data of a MDR transporter.

No correlation could be outlined between the activity data and the $\log P$ values (Fig. 3) suggesting that $\log P$, although an important lipophilicity characteristic, is not linearly related to the activities of this series of compounds. In contrast to $\log P$, the hydrophobic indices generated by the CoMSIA models showed high correlations with activity; 'h' field alone produced a model with $q^2 = 0.712$ and $r^2 = 0.912$ (Table 2). This observation is in agreement with our previous studies of different classes of first-generation MDR modulators that pointed to the role of hydrophobicity as a space distributed molecular property for the modulating effect.^{23,24} It should, however, be noticed that, in contrast to the previous studies, the predictive ability of the hydrophobic field alone is relatively low ($p^2 = 0.27$ – 0.29 , Table 2) and the same has been detected in our 3D-QSAR study of anthranilamide analogs (average $p^2 = 0.31$).¹² This result confirms that, although an important structural property, hydrophobicity is not the only determinant for the inhibitory potency of the third-generation MDR modulators. The 3D-QSAR models outline the complex role of several structural properties (electrostatic, steric, HB-acceptor, and hydrophobic) for the inhibitory effect of the compounds. In this study, in contrast to the previous ones,^{12,13} a structurally more variable set of compounds have been analyzed including XR derivatives as well as originally synthesized compounds with smaller structures that do not contain an anthranilamide nucleus (Table 1). This requires a more sophisticated approach to the compounds' alignment that has been guided by flexible and pharmacophore superpositioning using the structure of Hoechst 33342 as a template and considering the pharmacophore pattern of the compounds binding to the H-site.²¹

Results of the flexible and pharmacophore overlays of the inhibitors suggest that the H-site could be a potential binding site for these compounds. Indeed, a number of experimental studies give evidence for a distinct binding site of Hoechst 33342 (H-site).^{25,26} From radioligand binding experiments, Martin et al. postulate that tariquidar and its analogs bind to the same site as Hoechst 33342.²⁷ Further, FRET experiments localize the H-site

in the transmembrane part of P-gp within the cytoplasmic membrane leaflet at 10.5–14.5 Å above the membrane surface.²⁸ Neither of these (nor mutagenesis) studies, however, point to particular amino acids involved in the H-site. Our recent results on identification of P-gp binding sites using its homology model demonstrate the presence of a number of binding pockets in the transmembrane related regions of the protein thus suggesting possibility for the same, overlapping or closely located binding sites of P-gp substrates and inhibitors.²⁹ In the present study this assumption is supported by the fact that in the mostly produced overlays a good correspondence has been observed between the functional groups of the inhibitor structures and the main points (H_2 , H_3 , A_2 , D_2) involved in the pharmacophore pattern of drugs that interact with the H-site of P-gp.²¹ For the inhibitors of template 1 the inhibitory effect can be mainly related to the amide group and attached to it the R_2 substructure. This part is rather flexible and strongly deviates from the part overlapped on Hoechst 33342 (Fig. 5). This implies the possibility of binding to an additional site of the protein and directs to a possible explanation of how these substances exert their remarkably high inhibitory effect on the P-gp function.

The inhibitory effect of the compounds of template 2 that interact with the H-site could be explained by a higher binding affinity compared to Hoechst 33342 and could probably be related to functional groups and atoms not present in the Hoechst 33342 structure. In the particular series of inhibitors the tetrahydroisoquinoline part appears as either unsubstituted or 6,7-methoxysubstituted (Table 1). The differences in the inhibitory effects of the methoxy-substituted and -unsubstituted compounds suggest that this substructure may play a role for the inhibitory effect of the compounds. This has also been proven by the Free-Wilson analysis of the compounds that outlined a statistically significant contribution of the methoxy groups in positions 6 and 7 to the activity of the compounds (data not shown).³⁰ Another possibility appears from the analysis of the contour plots (Fig. 9B) that points to additional HB-acceptor interactions involving the heteroatom in the 3-quinoline substituted compounds, similarly to HB-acceptor interactions potentially performed by the $=\text{O}$ atom of the amide group in the compounds of template 1.

The 3D-QSAR models derived in this study are highly predictive. In contrast to the study of Labrie et al.¹³ and our previous study where the 3D-QSAR models have been validated by a split of the whole data set into training and test sets,¹² in this study the validation of the model is performed on an external test set that is even larger than the training set (30 vs 28 compounds). Additional predictions have been done based on the correlation between activity values of the overlapping compounds in our and Xenova Ltd set. Table 3 summarizes the data for the overlapping compounds. In the table the data are presented as taken from the publication of Roe et al.¹⁰ and the Xenova group Ltd patent.⁹ The corresponding pIC_{50} obtained in our assays is also shown. To cope with the differences in the values reported in

Table 3. Comparison of inhibition activity of the XR and WK compounds

Compound	Daunorubicin accumulation assay				Hoechst 33342 assay	
	Ref. 10		Ref. 9 ^a		PCA values	pIC ₅₀
	IC ₅₀ (nM)	pIC ₅₀	IC ₅₀ (nM)	pIC ₅₀		
XR9456	250 ± 25	6.60	300	6.52	6.58	6.29 ± 0.06
XR9544	87 ± 13	7.06	50	7.30	7.19	6.78 ± 0.09
XR9576	38 ± 18	7.42	64	7.19	7.32	—
XR9577	—	—	320	6.50	6.57	6.45 ± 0.07
XR9504	—	—	260	6.59	6.65	6.28 ± 0.23
Cyclosporin A	440 ± 230	6.36	—	—	6.42	5.85 ± 0.05
Verapamil	5800 ± 2200	5.24	—	—	5.39	5.18 ± 0.20
<i>Predicted activity values of the most active compounds</i>						
WK-X-51	—	—	—	—	7.24 ^b	—
XR9576	—	—	—	—	—	6.91 ^b 6.90 ^c

^a No error reported.^b Predicted from the PCA correlations (Fig. 10).^c Predicted by the 3D-QSAR model 'seha' (Table 2).

Refs. 9 and 10, a PCA analysis was performed and the activity of the compounds recalculated (Table 3). The obtained values were then correlated to those of the Hoechst 33342 assay. Figure 10 presents this correlation. As seen from the figure there is a very good correspondence between inhibitory effects of the overlapping data confirming that functional assays lead to correlated results.¹⁶ This allows, applying the regression equation fit, to predict the positions of the most active compounds in the assays—XR9576 from the XR-series and WK-X-51 from the WK-series. The predicted values of XR9576 are shown in the bottom part of Table 3. As seen from the table there is an excellent correspondence between the inhibitory potency of tariquidar in the Hoechst 33342 assay calculated from the experimental data correlations (pIC₅₀ = 6.91, Fig. 9) and predicted from the 3D-QSAR model (pIC₅₀ = 6.90, Fig. 8B). The expected activity of the strongest compound in the series WK-X-51 in daunorubicin accumulation assay is pIC₅₀ = 7.24, suggesting its high inhibitory potency also in this assay.

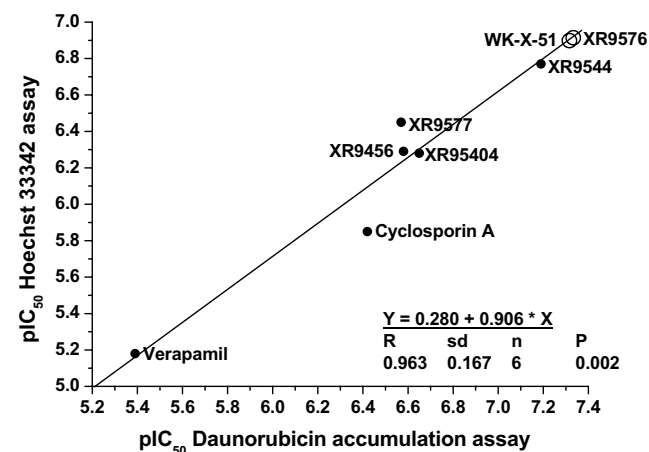


Figure 10. Correlation between the inhibitory effects of the compounds that overlapped in the Hoechst 33342 and daunorubicin accumulation assays^{9,10}; the predicted activities of XR9576 and WK-X-51 calculated from the regression equation are shown as open circles.

In conclusion, in this study we combined functional assays and molecular modeling approaches to a series of novel third-generation P-gp inhibitors. The results demonstrate that the functional assays at different substrate concentrations can be used to decide on the type of inhibition and thus, on the potential binding site of the inhibitor on the transport protein. The molecular modeling approaches direct to the possible way of binding and help in identification of the functional groups and atoms important for the inhibition potency. The 3D-QSAR models derived can support prediction and rational design of new P-gp inhibitors. Some of the newly synthesized inhibitors (WK-X-51, WK-X-34, WK-Y-27, WK-X-52) possess high inhibitory effects and may represent suitable candidates for further pharmacological studies.

4. Experimental

4.1. Chemicals

The novel tetrahydrosioquinoline-ethyl-phenyl-amine based MDR inhibitors, as well as the XR derivatives XR9456, XR9054, XR9577, and XR9544, have been recently synthesized in our laboratory.¹⁷ Stock solutions (10 mM) were prepared in DMSO. The cytostatic compound doxorubicin was kindly provided by Medac (Hamburg, Germany). All other chemicals were obtained from Sigma Chemicals (Taufkirchen, Germany) unless otherwise stated.

4.2. Cell culture

Human ovarian carcinoma cell lines A2780 and its MDR1 (P-gp) overexpressing counterpart A2780Adr were purchased from ECACC (European collection of animal cell cultures, No. 93112520 [A2780adr] and No. 93112519 [A2780], United Kingdom). These cell lines were cultured in RPMI-1640 medium supplemented with 10% fetal bovine serum, 50 µg/ml streptomycin, 50 U/ml penicillin G, and 365 µg/ml L-glutamine. Cells were incubated at 37 °C in a humidified atmosphere con-

taining 5% CO₂. Cells were grown to 80–90% confluence and treated with trypsin–EDTA before subculturing. To conserve P-gp overexpression and maintain resistance every fifth passage, doxorubicin (0.1 µM final concentration) was added to the cell culture medium.

4.3. Hoechst 33342 assay

Cells were grown under standard conditions in T75- or T175-flasks. After reaching confluence of approximately 80%, cells were harvested by short trypsinization (0.05% trypsin/0.02% EDTA). Pelleted cells were resuspended in fresh culture medium and counted with a Casy I Modell TT cell counter (Schaerfe System GmbH, Reutlingen, Germany). Cells were washed three times with Krebs–Hepes buffer and then were seeded into black 96-well plates (Greiner, Frickenhausen, Germany) at a density of approximately 30,000 cells in a volume of 90 µl per well. Then, 10 µl of various test compounds in different concentrations were added, resulting in a final volume of 100 µl per well. The prepared 96-well plates were kept under standard conditions for 30 min. After this preincubation period, 20 µl of a 30 µM Hoechst 33342 solution which was protected from light were added to each well. Subsequently, fluorescence was measured immediately in constant time intervals (120 s) up to 16 min at an excitation wavelength of 365 nm and an emission wavelength of 450 nm using a 37 °C tempered BMG POLARstar microplate reader.

4.4. Calcein AM assay

Since many steps in the preparation of the Hoechst 33342 assay are identical to the protocol of the Calcein AM assay only the differences are outlined: The cells were prepared in the same manner, but seeded into colorless 96-well plates (Greiner, Frickenhausen, Germany) at a density of approximately 30,000 cells per well (one well including 90 µl cell suspension and 10 µl test compound solution). After the preincubation period with the test compounds, 33 µl of a 1.25 µM Calcein AM solution which was protected from light was added to each well.

The fluorescence was detected immediately at constant time intervals (120 s) up to 46 min at an excitation wavelength of 485 nm and an emission wavelength of 520 nm applying a 37 °C tempered BMG POLARstar microplate reader.

4.5. Assay data analyses

The 96-well plate was divided into two parts: the main part including 64 wells was provided with cells, the second part containing of the remaining 32 wells was only filled up with Krebs–Hepes buffer. The 33 wells localized in the 1st, 4th, 7th, and 10th column of the 12 columns of the 96-well plate were defined as ‘background wells’. Each modulator or substrate concentration was added to three wells containing one ‘background well’ and two wells including cells. The fluorescence measured in the ‘background wells’ was subtracted from the fluorescence measured in the corresponding wells which were

supplemented with cells. These data were used for the following analyses.

The fluorescence-data points were measured up to 16 and 46 min for Calcein AM and Hoechst 33342, respectively, and the slopes were calculated by linear regression and used as dependent parameters. From these data concentration–response curves were generated by nonlinear regression using the 4-parameter logistic equation with variable Hill slope (GraphPad Prism 5.0 software, San Diego, CA). For less active compounds the top-value of the concentration–response curve was defined by a control containing 10 µM XR9577, that led to total inhibition of P-gp.

Under the assay conditions with sub-saturating substrate concentrations, the ratio of intracellular (c_{in}) to extracellular (c_{out}) substrate concentration depends on the ratio of pumping speed to the rate of passive diffusion (k^*) as follows (for the development of this relationship, see Ref. 31):

$$\frac{c_{in}}{c_{out}} = \frac{1}{1 + k^*} = \frac{Bottom}{Top}$$

Bottom corresponds to the minimal fluorescence without inhibition of P-gp and *Top* denotes the maximal fluorescence obtained with full inhibition of P-gp. Thus, the determined IC₅₀ values agree with 50% inhibition of P-gp only at very high pump rates compared to the speed of passive diffusion and therefore have to be considered as apparent inhibition constants. However, as long as the expression and resistance levels remain constant, the apparent IC₅₀ values can be used for comparative purposes.

4.6. Log *P*, p*K*_a, and PCA calculations

The log *P* (log *D*) and p*K*_a values of the compounds were calculated with the program ACD.¹⁹ For the p*K*_a values the ‘apparent constants’ approach is applied that mimics the experimental order of protonation and determines the p*K*_a values, which can be really experimentally measured in water solution. Statistical analyses including PCA were performed using SPSS (version 12.0 for Windows).³²

4.7. Molecular modeling methods

Molecular modeling was carried out with the programs MOE (Molecular Operating Environment)³³ and SYBYL.³⁵ The conformational analysis was performed by simulated annealing in SYBYL and by the stochastic search in MOE. In the simulated annealing repeated heating and cooling of a molecule is simulated to cover the conformational space. In the stochastic search a random rotation of all bonds (including also ring bonds) and subsequent atom coordinates perturbation is performed (similar to scrambling of the absolute coordinates of the atoms) followed by the structure minimization. The force field methods used were Tripos and MMFF94s. The AM1 semiempirical method (MOPAC³⁴) was applied for geometrical optimization and

calculation of the partial atomic charges of the molecules. 3D-QSARs were derived with the CoMFA and CoMSIA approaches as implemented in SYBYL.

4.8. 3D structure generation

As no X-ray data of Hoechst 33342 were available, the energy minimum conformers of the compound were generated from the sketched and minimized structure of Hoechst 33342 (Tripos force field, $0.05 \text{ kcal mol}^{-1} \text{ \AA}^{-1}$ gradient, no charges). Two techniques were applied: simulated annealing and stochastic search. Simulated annealing was performed with 100 cycles, 2000 K initial temperature for heating for 2000 fs equilibration, 0 K target temperature for 5000 fs annealing time, and exponential annealing function. The obtained 100 local minima were then optimized by the semiempirical method AM1 (full optimization, precise convergence, 'xyz' keyword, MOPAC 6.0³⁴). In the stochastic search the MMFF94s force field was used with the default MOE settings. To ensure a better covering of the conformational space, the following parameters were increased: energy cutoff 10 kcal/mol, failure limit 200 (contiguous number of attempts to generate a new conformation), RMS tolerance 0.5, iteration limit 20,000, minimization iteration limit 2000. Both techniques produced similar results. Four clusters of Hoechst 33342 conformations were identified and the lowest energy conformer of each cluster was taken for further analysis. The conformers differed in the relative orientation of the benzimidazole rings toward each other. In one pair of conformers the imidazole nitrogens ($-\text{NH}$ and $=\text{N}-$) in both benzimidazole rings had opposite orientations (just as shown in Fig. 5). In another pair, vice versa, the benzimidazole ring with the attached piperazine was rotated by 180° . The four conformers had AM1 heats of formations in the interval from 142.1 kcal/mol to 145.1 kcal/mol. As the heats of formation were very close, to decide on the best conformer, all four conformers of Hoechst 33342 were used as templates for identification of its pharmacophore pattern. The conformer with the lowest heat of formation was selected for further analyses.

Similarly to Hoechst 33342 the structures of the XR and WK compounds were sketched and a stochastic search was performed with all of them. The settings were the same as used for Hoechst 33342 (see above) but additionally rotation of the amide bonds was allowed. The most appropriate conformations were selected based on the flexible alignment results generated by FlexS (see details below) and a subsequent refinement by the pharmacophore search in MOE. The structures were then minimized again with Tripos force field ($0.05 \text{ kcal mol}^{-1} \text{ \AA}^{-1}$ gradient, no charges) keeping the pharmacophore template as an aggregate and afterwards optimized with AM1 full optimization, precise convergence, 'xyz' and 'mmok' keywords.

4.9. FlexS alignments

For a given template molecule FlexS²⁰ predicts conformations and orientations of the ligands relative to the

template. The algorithm treats the template molecule as rigid. In the capacity of a template the lowest energy conformer of Hoechst 33342 was used (see above). The overlays of the compounds were produced by 'Flexible superposition'. This option combines the conformational search with an alignment. The conformational search generates a new conformation in two steps: (i) by selection and placement of a base fragment (of the current ligand) on the template specified; (ii) by incremental build up of the remaining part of the ligand and subsequent scoring of the generated conformation for estimation of the superposition quality.

FlexS runs were performed with MMFF94s force field and charge calculation method MMFF94. Different numbers of alignments per ligand (from minimum 30 to maximum 100) were experimented and the minimum volume overlap of 0.3 (default 0.6) was set to ensure a higher variety in the resulting overlays. Different conformers of the same compounds were processed (from 1 to up to 4 conformers per structure) to additionally force the variety in the produced overlays. In most cases similar overlays were recorded. The final alignment of the structures applied in the subsequent 3D-QSAR analyses was done as described in Section 2.

4.10. CoMFA and CoMSIA specifications

The standard settings were used in the CoMFA calculations³⁵: 2 \AA regular grid size in all three directions within the automatically created grid box with 4 \AA extension beyond the van der Waals volume of the overlaid molecules, sp^3 carbon probe with +1 charge, a distance dependent ($1/r$) dielectric constant. The following fields were calculated in CoMFA: steric (s), electrostatic (e), both (b), and hydrogen bond (h-bnd). The AM1 point charges were used for calculation of the electrostatic fields. The standard energetic cutoff value of 30 kcal/mol with no electrostatic interactions at bad steric contacts was used. The threshold column filtering was set to 1.0 kcal/mol. In CoMSIA the following similarity indices fields were calculated: steric (s), electrostatic (e), hydrophobic (h), hydrogen bond donor (d), hydrogen bond acceptor (a), hydrogen bond donor (d), and donor-acceptor (da) with the default attenuation factor of 0.3 in the same grid box as used for CoMFA. A common probe atom with 1 \AA radius and charge, hydrophobicity, and hydrogen bond property of +1 was used. The indices were evaluated according to the usual CoMSIA protocol with 1.0 column filtering.

The CoMFA and CoMSIA QSAR equations were calculated by the PLS (Partial Least Squares) method. The internal predictive power of the models was evaluated by LOO (Leave-One-Out) cross-validation using the cross-validated squared correlation coefficient q^2 , the optimal number of components n , and the predictive sum of squares S_{PRESS} .

The linear regression fit was qualified by the squared correlation coefficient r^2 and the standard error of estimate s . The external predictive power of the obtained models was estimated by the predictive squared correla-

tion coefficient r^2_{pred} .³⁵ Additionally a parameter called p^2 was calculated as follows³⁶:

$$p^2 = 1 - \frac{\sum_{i,j} [(p_i - p_j) - (m_i - m_j)]^2}{\sum_{i,j} (m_i - m_j)^2},$$

where p_i , p_j were predicted activities and m_i , m_j were measured activities. It describes the predictive power of the model based on the pair wise predicted and observed activity differences and is therefore independent of the additive constants like means of the training and test sets.

The visualization of the regions where variability in the molecular properties explained best the biological activity differences made use of the SD * Coefficients contour fields. The selection of the contour levels for the favorable and unfavorable interactions considered the distribution of each SD * Coefficients field according to the recommendations published in Ref. 22.

Acknowledgments

I.K. Pajeva and M. Wiese thank the Alexander von Humboldt Foundation for the financial support (BUL/1021057 STP). I.K. Pajeva acknowledges also the partial support of the NSF-Bulgaria (Grant L-1416).

References and notes

- Juliano, R. L.; Ling, V. *Biochim. Biophys. Acta* **1976**, *455*, 152.
- Thomas, H.; Coley, H. M. *Cancer Control* **2003**, *10*, 159.
- Robert, J.; Jarry, C. *J. Med. Chem.* **2003**, *46*, 4805.
- Krishna, R.; Mayer, L. D. *Eur. J. Pharm. Sci.* **2000**, *11*, 265.
- Mistry, P.; Stewart, A. J.; Dangerfield, W.; Okiji, S.; Liddle, C.; Bootle, D.; Plumb, J. A.; Templeton, D.; Charlton, P. *Cancer Res.* **2001**, *61*, 749.
- Walker, J.; Martin, C.; Callaghan, R. *Eur. J. Cancer* **2004**, *40*, 594.
- Martin, C.; Berridge, G.; Mistry, P.; Higgins, C.; Charlton, P.; Callaghan, R. *Br. J. Pharmacol.* **1999**, *128*, 403.
- Fox, E.; Bates, S. E. *Expert Rev. Anticancer Ther.* **2007**, *7*, 447.
- Ryder, H.; Ashworth, P. A.; Roe, M. J.; Brumwell, J. E.; Hunjan, S.; Folkes, A. J.; Sanderson, J. T.; Williams, S.; Maximen, L. M. Anthranilic acid derivatives as multi drug resistance modulators. WO98/17648, April 30, 1998.
- Roe, M.; Folkes, A.; Ashworth, P.; Brumwell, J.; Chima, L.; Hunjan, S.; Pretswell, I.; Dangerfield, W.; Ryder, H.; Charlton, P. *Bioorg. Med. Chem. Lett.* **1999**, *9*, 595.
- Martin, C.; Berridge, G.; Higgins, C. F.; Mistry, P.; Charlton, P.; Callaghan, R. *Mol. Pharmacol.* **2000**, *58*, 624.
- Globish, C.; Pajeva, I. K.; Wiese, M. *Bioorg. Med. Chem.* **2006**, *14*, 1588.
- Labrie, P.; Maddaford, S. P.; Fortin, S.; Rakhit, S.; Lakshmi, P.; Kotra, L. P.; Gaudreault, R. C. *J. Med. Chem.* **2006**, *49*, 7646.
- Jekerle, V.; Klinkhammer, W.; Reilly, R. M.; Piquette-Miller, M.; Wiese, M. *Cancer Chemother. Pharmacol.* **2007**, *59*, 61.
- Jekerle, V.; Klinkhammer, W.; Scollard, D. A.; Breitbach, K.; Reilly, R. M.; Piquette-Miller, M.; Wiese, M. *Int. J. Cancer* **2006**, *119*, 414.
- Müller, H.; Klinkhammer, W.; Globisch, C.; Kassack, M. U.; Pajeva, I. K.; Wiese, M. *Bioorg. Med. Chem.* **2007**, *15*, 7470.
- Klinkhammer, W.; *Design, Synthese und 3D-QSAR neuer tiger P-gp-Modulatoren*, Ph.D. thesis, University of Bonn, **2006**; http://deposit.ddb.de/cgi-bin/dokserv?idn=981124488&dok_var=d1&dok_ext=pdf&filename=981124488.pdf.
- Segel, I. H. *Enzyme Kinetics*; John Wiley and Sons: New York, 1976.
- ACD/Labs, version 5.09, ACD pKa DB Advanced Chemistry Development, Inc., Toronto, ON, Canada.
- FlexS, SYBYL 6.9 version; Tripos Inc., 1699 South Hanley Road, St. Louis, MO 63114-2917.
- Pajeva, I. K.; Globisch, C.; Wiese, M. *J. Med. Chem.* **2004**, *47*, 2523.
- Pajeva, I. K.; Wiese, M. *Quant. Struct.-Act. Relat.* **1999**, *18*, 369.
- Pajeva, I.; Globisch, C.; Fleischer, R.; Tsakovska, I.; Wiese, M. *Med. Chem. Res.* **2005**, *14*, 106.
- Pajeva, I. K.; Wiese, M. *J. Med. Chem.* **1998**, *41*, 1815.
- Shapiro, A. B.; Ling, V. *Eur. J. Biochem.* **1997**, *250*, 122.
- Safa, A. R. *Curr. Med. Chem. Anticancer Agents* **2004**, *4*, 1.
- Martin, C.; Berridge, G.; Higgins, C. F.; Mistry, P.; Charlton, P.; Callaghan, R. *Mol. Pharmacol.* **2000**, *58*, 624.
- Qu, Q.; Sharom, F. J. *Biochemistry* **2002**, *41*, 4744.
- Globish, C.; Pajeva, I. K.; Wiese, M. *ChemMedChem.*, in press.
- Müller, H. Funktionelle Untersuchungen des ABC-Transporters P-Glykoprotein, Ph.D. thesis, University of Bonn, 2007.
- Garnier-Suillerot, A.; Marbeuf-Gueye, C.; Salerno, N.; Loetchutin, C.; Fokt, I.; Krawczyk, M.; Kowalczyk, T.; Priebe, W. *Curr. Med. Chem.* **2001**, *8*, 51.
- SPSS, version 12, SPSS, Chicago IL, USA.
- MOE 2002.03 (Molecular Operating Environment), Chemical Computing Group, 1010 Sherbrooke Street West, Suite 910; Montreal, Que., Canada H3A 2R7.
- MOPAC 6, (QCPE No. 445): Department of Chemistry, Indiana University, Bloomington, IN 47405, USA.
- SYBYL 6.9–7.3 versions; Tripos Inc., 1699 South Hanley Road, St. Louis, MO 63114-2917.
- Silverman, D. *Quant. Struct.-Act. Relat.* **2000**, *19*, 237.